SPIE—The International Society for Optical Engineering

Optical Techniques in Fluid, Thermal, and Combustion Flow

10–13 July 1995
San Diego, California

Volume 2546

Interferometric Tomographic Measurement of an Instantaneous Flow Field Under Adverse Environments

Enxi Yu and Soyoung Stephen Cha

The University of Illinois at Chicago, Department of Mechanical Engineering, Chicago, IL 60607

Alpheus W. Burner

NASA Langley Research Center, Hampton, VA 23681

ABSTRACT

Measurement of an instantaneous flow field by interferometric tomography, that is, reconstruction of a three-dimensional refractive-index field from multi-directional projection data, has been conducted. In order to simulate the expected experimental arrangement at a wind tunnel, reconstructions are made from a restricted view angle less than 40 degrees and incomplete projections. In addition, appreciable ambient air and experimental setup disturbances are present. A new phase-stepping technique, based on a generalized phase-stepping approach of a four-bucket model, is applied for expeditious and accurate phase information extraction from projection interferograms under the harsh environments. Phase errors caused by the various disturbances, which can include ambient refractive-index change, optical component disturbance, hologram repositioning error, etc., are partially compensated with a linear corrective model. A new computational tomographic technique based on a series expansion approach was also utilized to efficiently deal with arbitrary boundary shapes and the continuous flow fields in reconstruction. The results of the preliminary investigation are encouraging; however, the technique needs to be further developed in the future through refinement of the approaches reported here and through hybridization with previously developed techniques.

Keywords: interferometry, tomography, phase stepping

1. INTRODUCTION

Interferometric tomography is a technique for reconstructing three-dimensional (3-D) refractive-index fields from two-dimensional multi-directional interferometric projection data. It can thus provide means for capturing spatial distributions of physical properties related to refractive-index, including density, temperature, and gas species. Measurements of 3-D flow fields can be the most important nature of interferometric tomography. Its detection is nonintrusive and very sensitive, being based on remote interferometric sensing. It has a potential to offer good spatial resolution and measurement accuracy if the problems of limited projection data acquisition and appreciable external noise can be overcome. Interferometric tomography needs continual technology enhancement to be a practical diagnostic tool in order to provide reliable 3-D field reconstruction under these adverse environments.

The typical limiting conditions in data acquisition are incomplete projection and restricted angular scanning as demonstrated in Fig. 1. In practical wind tunnel applications of interferometric tomography, test models and facility enclosures are frequently present inside and outside the flow field to be reconstructed. The opaque objects restrict the angular scanning of the field or block a portion of the probing rays, allowing only a partial data set. The interferometric data are thus mostly discontinuous and nonuniform in sampling. These in turn pose the formidable challenge of reconstruction from a limited data set. The nature of this ill-posed problem and some efforts to resolve it have been addressed in previous publications [1-3]. The ill-posed reconstruction is sensitive to experimental noise and can produce serious distortions in reconstruction.

Another challenge in interferometric tomography is to instantaneously obtain many multi-directional projection interferograms with as wide a scanning angle as possible and to process these interferograms for phase information extraction in a quick and accurate manner. The instantaneous scanning of flow fields is necessary when transient phenomena are captured. This challenge can be met by utilizing diffuse illumination for holographically recording and projecting a flow field [4,5] and by applying a phase-stepping technique [6] with a restricted scanning angle. However, it is likely that phase unwrapping errors will arise, owing to the speckle noise produced by the diffuse illumination and the harsh environments in practical measurements, especially in aerodynamic testing. Efficient mechanisms for noise elimination and correction are thus required.

In interferometric tomography, the projection data of a 3-D flow field are usually obtained with a double-exposure holographic technique. In this interferometric method, the field is recorded before and after the disturbance on a single holographic plate. When the hologram is reconstructed, the interference fringes which appear are caused by interference between the disturbed and undisturbed fields. These fringe patterns represent the optical phase changes between the two exposures.

When a projection of a two-dimensional slice of the 3-D field is considered, the projection data can be expressed as a function of the scanning angle θ and the distance ρ from the optical axis as shown in Fig. 1. The projection data $g(\rho,\theta)$ is the line integral of the refractive-index difference $f(x,y)$ between two exposures when a refractionless limit is assumed. It can be described by Eq. (1).

$$g(\rho,\theta) = N(\rho,\theta)\,\lambda = \int_{ray} f(x,y)ds = \int_{ray} [n(x,y) - n_0]ds\,, \tag{1}$$

where ds, $N(\rho,\theta)$, and λ are the differential element of a probing ray, fringe order number, and wavelength of the probing beam, respectively. $n(x,y)$ and n_0 are refractive indices of the disturbed and undisturbed field. The tomographic reconstruction thus corresponds to inversion of the line integral transform, or equivalently, the two-dimensional Radon transform [2]. In the case of a 3-D field, it can be built by stacking up sliced sections of reconstructed two-dimensional fields.

Briefly, interferometric tomography consists of three major steps. First, multi-directional projections of a flow field are obtained, which yield many two-dimensional interferograms. Second, these interferograms need to be processed to obtain optical pathlength data corresponding to individual probing rays. Third, the field is then reconstructed through the numerical inversion of the line integral transform to yield optical pathlength data of projections. In the following sections, we will discuss the approaches one by one, which were employed for these steps in our experiment.

2. EXPERIMENTAL SETUP

The experiment reported here was performed as a preliminary test to confirm the capabilities of our technique and to identify its associated problems before applying it to actual aerodynamic measurements in a high-speed wind tunnel. For this reason, the mock-up test was designed at a laboratory with a flow produced by a thermal plume generator. Figure 2 shows the schematic of the flow field generator and a test model. The distance between the top of the model and the top of the generator surface was about 1.2 *cm*. Two slender cartridge heaters of different strength, 150 W and 300 W were installed in the generator horizontally in parallel to produce a flow cross-section close to an elliptical shape of 2.5"×3.5". The flow intensity was controlled by adjusting the input voltage to the heaters. The test model further distorted the flow cross-section of its nearby region where the reconstructions were conducted. Two thermocouple rakes with four thermocouples on each were installed on both sides of the test model for comparison with interferometric tomographic reconstruction. Figure 3 shows the experimental arrangement for

instantaneously recording multi-directional projection information of a transient flow field. The setup basically utilizes diffuser-illumination of test fields, holographic interferometric recording of 3-D fields, and a phase-stepping technique for projection data extraction. The system was designed to provide the solutions to the challenging tasks as discussed in Section 1. The exposure time for the argon-ion laser (wavelength λ=514.5 *nm*) was controlled with an electronic shutter; however, for fast transient phenomena, a pulsed laser can be used.

In aerodynamic testing, it may be difficult to install many diffusers and holographic plates around a test section enclosure to provide a wide scanning angle in obtaining projection interferograms. In addition, the system is more complex. Our experimental setup was relatively simple, utilizing one diffuser of 14"×11" and one holographic recording area of 10"×4" that were placed along a single optical axis which allowed only a limited view angle of about 40 degrees. Two 5"×4" Agfa-Gevaert 10E56 holographic plates were mounted side by side in contact for the 10"×4" recording area. In our experiment dual reference beams that were very close to each other were employed for double-exposure hologram recording. The exposures were taken with and without the heaters on. The temperature of ambient air after the first exposure was continuously drifting around 26°C. During the recording, the data logger was synchronized with the laser beam shutter to simultaneously record the thermocouple values. The same reference beams were then used for holographic interferogram reconstruction. One of the reconstruction beams, however, was phase-stepped with a liquid-crystal phase retarder that was controlled by a digital signal generator. The experimental environments were too harsh to apply conventional phase-stepping techniques[7], thus the calibration curve of the phase retarder was inconsequential in detecting phase-stepping values. Since the phase-stepping continually fluctuated around the values commanded by the phase retarder owing to the appreciable contribution by the external disturbances, a new approach was adopted. For implementation, two-dimensional images of vertical Young's fringes formed by the two reconstruction beams were magnified by a cylindrical lens and captured by a CCD camera simultaneously with phased-stepped projection interferograms as shown in Fig. 3. The uneven phase-stepping values were then extracted as explained later. To the best knowledge of the authors, this may be the first effort to directly extract phase-stepping values based on Young's fringe analysis for application to severely disturbing environments. Despite the continual drifting and jitter of the Young's fringe pattern, accurate extraction of phase-stepping values was possible.

The reconstructed 3-D holographic image was scanned to obtain multi-directional projection interferograms with a rotary rail-mounted imaging system whose axis was centered on the middle of the flow field. A telecentric system was employed to relay the projection images to a CCD camera. The flow field was scanned for 41 projections over a scanning angle of 40 degrees, 20 degrees from the normal to the hologram in both directions with an increment interval of one degree. The field could be projected only partially near both extreme sides of scanning owing to the finite sizes of the diffuser and hologram. The effective scanning angle, which is equivalent to the value limited to full-field projections, was thus only about 35 degrees. For each projection, four interferograms were obtained, each of which was about 90 degrees apart in phase-stepping. The projection image acquisition, which involves the operations of two CCD cameras and frame grabber and the digital signal generator for phase-stepping, were controlled by a computer.

3. PHASE INFORMATION EXTRACTION

3.1 Extraction of phase-stepping values

As discussed earlier, four interferograms were recorded for each projection, with uneven phase-stepping values owing to the appreciable external disturbances of unknown magnitude. The procedure for accurately extracting phase-stepping values from observed Young's fringes as well as some processing examples are demonstrated below.

(1) A two-dimensional Young's fringe pattern $I_{x,y}$, where (x,y) is a pixel position with the y-axis along the fringe direction, can be compressed to a one-dimensional image I_x^c,

$$I_x^c = \frac{1}{N}\sum_{y=1}^{N} I_{x,y} \tag{2}$$

where N is the number of pixels (240 in our case) in the y-direction. Figures 4(a) and (b) show an example of a two-dimensional fringe gray scale with the corresponding coordinates and compressed one-dimensional image. This processing reduces substantially the noise that appears in the two-dimensional image.

(2) In general, the higher the intensity, the greater the noise level including laser speckle. Thus the locations of fringe minima rather than maxima are used to determine fringe displacement. The intensity data I_x^c is thus inverted as seen in Fig. 4(c) before determining the minima location.

(3) The inverted one-dimensional fringe pattern is then thresholded and the peak displacement Δx of the arch-shaped fringe is determined by finding its gray-scale centroid. The fringe spacing L can also be found from the detection of two neighboring peaks. The extracted values of Δx and L, which correspond to Fig. 4(c) are shown in Fig. 4(d).

(4) The phase-stepped value $\Delta\varphi$ from a reference fringe pattern can be found by

$$\Delta\varphi = 2\pi\frac{\Delta x}{L}. \tag{3}$$

3.2 Extraction of Optical Pathlength Data

Each projection of a flow field produced four phase-stepped interferograms with uneven phase-stepping values. After determining the phase-stepping values as described in Section 3.1, the phase information or equivalently the optical pathlength data of each projection can be found by applying a generalized multi-bucket phase-stepping model[8] as briefly discussed below.

An interferogram can be expressed by

$$I_i(x,y) = B(x,y) + A(x,y)\cos[P(x,y) + \Delta\psi(x,y) + \Delta\varphi_i] \tag{4}$$

where $I_i(x,y)$, B(x,y) and A(x,y) are the irradiance of a phase-stepped interferogram, background irradiance, and modulation amplitude, respectively. P(x,y) is the phase value to be extracted corresponding to the flow field change during two holographic exposures, $\Delta\psi(x,y)$ is the phase change owing to external disturbances of the ambient air and optical setup during holographic recording and reconstruction, and $\Delta\varphi_i$ is the phase-stepping value relative to a reference frame. The subscript i represents the phase-stepping sequence with maximum value of N. In our processing the reference frame corresponded to the first frame with $\Delta\varphi$=0. Figure 5 demonstrates phase-stepped interferograms at a projection direction normal to the hologram. The top surface of the flow generator and the thermocouple rakes are also shown. Note that the fringe pattern moves as the phase-stepping increases.

Equation (4) can be rewritten as

$$I_i(x,y) = B(x,y) + A_1(x,y)\cos(\Delta\varphi_i) + A_2(x,y)\sin(\Delta\varphi_i) \tag{5}$$

where

$$\begin{aligned} A_1(x,y) &= A(x,y)\cos[P(x,y) + \Delta\psi(x,y)] \\ A_2(x,y) &= -A(x,y)\sin[P(x,y) + \Delta\psi(x,y)]. \end{aligned} \tag{6}$$

With known $\Delta\varphi_i$ and measured intensity data $I_i(x,y)$, the unknowns of $B(x,y)$, $A_1(x,y)$, and $A_2(x,y)$ in Eq. (5) can be determined as long as more than three phase-stepped frames are obtained. In general, the more frames are collected , the better noise suppression can be made. When an ordinary least square method [9] is applied, the estimated values become the solution of Eq. (7).

$$\begin{bmatrix} N & \sum_{i=1}^{N}\cos(\Delta\varphi_i) & \sum_{i=1}^{N}\sin(\Delta\varphi_i) \\ \sum_{i=1}^{N}\cos(\Delta\varphi_i) & \sum_{i=1}^{N}\cos^2(\Delta\varphi_i) & \sum_{i=1}^{N}\sin(\Delta\varphi_i)\cos(\Delta\varphi_i) \\ \sum_{i=1}^{N}\sin(\Delta\varphi_i) & \sum_{i=1}^{N}\sin(\Delta\varphi_i)\cos(\Delta\varphi_i) & \sum_{i=1}^{N}\sin^2(\Delta\varphi_i) \end{bmatrix} \begin{bmatrix} B \\ A_1 \\ A_2 \end{bmatrix} = \begin{bmatrix} \sum_{i=1}^{N} I_i \\ \sum_{i=1}^{N} I_i\cos(\Delta\varphi_i) \\ \sum_{i=1}^{N} I_i\sin(\Delta\varphi_i) \end{bmatrix}. \tag{7}$$

Once $A_1(x,y)$ and $A_2(x,y)$ can be determined, the unadjusted phase $P_u(x,y)$ of $P(x,y)$ and $\Delta\psi(x,y)$ can be obtained by Eq. (6).

$$P_u(x,y) = P(x,y) + \Delta\psi(x,y) = \tan^{-1}\left[\frac{A_2(x,y)}{A_1(x,y)}\right]. \tag{8}$$

The information extracted from Eq. (8) poses a problem of 2π ambiguity, that is, it can provide only wrapped phase values. The unwrapped information can be obtained by applying an appropriate phase-unwrapping technique such as a local gradient technique [7]. Figure 6 shows a plot of the unadjusted unwrapped-phase information extracted from the interferograms in Fig. 5 for the horizontal line 0.95 *cm* above the flow generator surface, which was processed according to the technique presented above.

The phase values obtained from Eq. (8) contain an unknown disturbance factor of $\Delta\psi(x,y)$. This fact can be clearly seen in Fig. 6. For our experiment, the phase values outside the flow region boundaries of $P(x,y)$ should be zero. Based on this knowledge, we can provide some means for correcting the unknown disturbance. Since only the zero phase boundary conditions are available at both ends of the field projection, a first approximation is made by assuming a linear correction model for $\Delta\psi(x,y)$. By this method, the phase value to be extracted, the adjusted value P, was calculated from Eq. (9) for each specific cross-section of the field.

$$\begin{aligned} P(x) &= P_u(x) - (\Delta_1 + ky) \\ &= P_u(x) - [\Delta_2 + k(L_e - y)] \\ k &= (\Delta_1 - \Delta_2)/L_e \end{aligned} \tag{9}$$

where Δ_1 and Δ_2 are the phase deviations from the null boundary value at both ends of the boundary projection as shown in Fig. 6. L_e and k are the field projection length and deviation slope, respectively. Near the two extreme scanning angles, Δ_1 or Δ_2 only is available due to the finite sizes of the diffuser and hologram. For the correction of these cases (11 out of 41 view angles), extrapolated values of the deviation slope were employed. The slope k can be collected with respect to the projection angle θ for the cases where both boundary deviations are available. The known k-values can than be curve-fitted as a function of θ to provide extrapolation.

4. COMPUTATIONAL TOMOGRAPHIC RECONSTRUCTION

The phase information extracted from projection interferograms can be converted to optical pathlength data $g(\rho,\theta)$ and then the flow field can be reconstructed as in Eq. (1). For computational tomography, a series expansion

method based on nonlocal basis functions was employed. In a series expansion method, the field $f(r,\phi)$ to be reconstructed is approximated by a finite series.

$$f(r,\phi)=\sum c_i\, b_i(r,\phi) \tag{10}$$

where $b_i(r,\phi)$ are the basis functions and c_i are the corresponding coefficients. The domain of definition of a basis function can be in the nonlocal entire region or a local partial region [2]. The line integral transform is linear. Here the transform and its inversion can be performed on a term-by-term basis.

$$g(\rho,\theta)=\sum c_i\, a_i(\rho,\theta) \tag{11}$$

where $a_i(\rho,\theta)$ is the line integral transform of $b_i(r,\phi)$. In series expansion, the functional values of b_i and a_i are known. If discrete data points of $g(\rho,\theta)$ are measured, c_i can thus be found from Eq. (11) by solving the redundant linear algebraic equations, i. e., ordinary least square method. With known c_i, the flow field can then be reconstructed with Eq. (10).

Most series expansion methods deal with a circular or rectangular field shape. As indicated earlier, the flow cross-section in our experiment differs from these previous ones, being close to an ellipse. A new approach was thus attempted, which is termed the curvilinear coordinate method. The method utilizes orthogonal polynomials in the radial direction and circular harmonics in the azimuthal direction. The orthogonal polynomials can be defined only in the interval between the boundaries and the flow region. The shapes of the flow field and the opaque model can thus be arbitrary but need to be specified as input. In our reconstruction, we employed an elliptical shape for the flow region. Our approach needs further refinement and details will be published later.

Once the refractive-index field, $f(x,y)=n(x,y)-n_0$, is reconstructed, it can be converted to related physical properties. In our experiment, the temperature field was found with Eq. (12), giving the relationship between refractive-index n and temperature T of air at λ=514.5 *nm* [4].

$$n-1=\frac{2.94036\times10^{-4}}{1+3.69203\times10^{-3}\,T} \tag{12}$$

where T is in Celsius. The refractive-index n_0 was calculated with the field temperature during the first exposure of 26.7°C. Figures 7 and 8 show two typical cross-sections of reconstruction: one 9.5 *mm* above the flow generator, without the opaque object and the other only a few pixels below the thermocouple tips, with the opaque test model blocking part of the projection.

No exact field is available for comparison with the interferometric tomographic reconstruction. Even though an elliptical flow cross-section was assumed, the exact shape is unknown. The reconstructed boundary values do not reduce to the ambient values of 26.7°C at some locations. The field might diminish very gradually beyond the assumed boundary, owing to the ambient fluctuation during the second exposure and the heating of the flow generator beyond the flow opening, or the phase information might be incorrectly adjusted by Eq. (9). The residual effects of these discrepancies might cause the nonuniform values at the field boundary. The reconstruction plane in Fig. 8 is slightly below the thermocouple tips. The comparison can not thus be exact. However, the eight thermocouple readings were 37.9°C, 45.5°C, 82.8°C, 147.4°C, 172.8°C, 171.8°C, 89.5°C, and 34.1°C while the corresponding reconstruction values at the points below the thermocouples were 31.7°C, 44.5°C, 78.8°C, 182.4°C, 176.8°C, 163.5°C, 99.2°C, and 30.7°C. As can be seen, the reconstructed temperatures agree quite well with the measured thermocouple readings except for the fourth value. This large discrepancy was found to be caused by a faulty thermocouple connection resulting in an erroneous measurement. When excluding the measured and

reconstructed values at this point, the average error of the remaining compared points is about 3.5% based on the difference between the maximum thermocouple temperature and the ambient temperature. When the harsh experimental environments, including the severely limited scanning angle, are considered, the reconstruction of the substantially asymmetric field appears to be reasonable as compared with the thermocouple measurements.

5. CONCLUSIONS

Interferometric tomography for reconstructing flow fields consists of three major steps: (1) capture of multi-directional projection interferograms, (2) accurate and reliable extraction of phase information, and (3) computational tomographic reconstruction. Here we presented some new approaches and corresponding results for individual steps. These techniques were developed for capturing instantaneous flow fields of arbitrary shape, under hostile environments involving external disturbances and limited-data conditions. Previously, some computational tomographic techniques have been developed to deal with ill-posed conditions, each of them addressing a different nature of reconstruction problems. Successful reconstructions with these techniques have been reported under limited conditions with an opaque model or scanning angle around 60 degrees. The reconstruction conditions here have been further restricted, with a scanning angle of about 35 degrees. A possible approach for further improvement would be to integrate the previously-developed typical techniques with the curvilinear coordinate method. Especially, the incorporation of the complementary field method [1] and the variable grid method [3] is believed to be very necessary to complement each other for performance enhancement under harsh environments expected in wind tunnel application. However, there will still exist a limit in scanning angle and opaque object size beyond which reliable reconstruction is not feasible.

In short, our results presented here are preliminary and limited, being based on the initial development of the computer programs. The techniques that have been discussed here need further refinement and testing in the future.

6. ACKNOWLEDGMENT

This research is supported by the National Aeronautics and Space Administration (Grant NAG-1-1594).

7. REFERENCES

1. S. S. Cha and H. Sun, "Tomography for reconstructing continuous fields from ill-posed multidirectional interferometric data", *Appl. Opt.*, Vol. 29, pp. 251-258, 1991.

2. S. S. Cha, "Interferometric tomography for three-dimensional flow fields via envelope function and orthogonal series expansion", *Opt. Eng.*, Vol. 27, pp. 557-567, 1988.

3. D. J. Cha and S. S. Cha, "Improvement of a series expansion approach to interferometric tomography via natural pixel decomposition", *Opt. Eng.*, Vol. 32, pp. 1685-1690, 1993.

4 C. M. Vest, *Holographic Interferometry*, Wiley, New York, 1979.

5. D. W. Sweeney and C. M. Vest, "Measurement of three-dimensional temperature fields above heated surfaces by holographic interferometry", *Int. J. Heat Mass Transfer*, Vol. 17, pp. 1443-1454, 1974.

6. B. Breuckmann and W. Thieme, "Computer-aided analysis of holographic interferograms using phase-shift method", *Appl. Opt.*, Vol. 24, pp. 2145-2149, 1985.

7. D. W. Robinson and G. T. Reid, *Interferogram Analysis*, Inst. Physics Pub., Philadelphia, 1993.

8. G. Lai and T. Yatagai, "Generalized phase-shifting interferometry", *J. Opt. Soc. Am. A*, Vol. 8, pp. 822-827, 1991.

9. J. V. Beck and K. J. Arnold, *Parameter Estimation in Engineering and Science*, Wiley, New York, 1977.

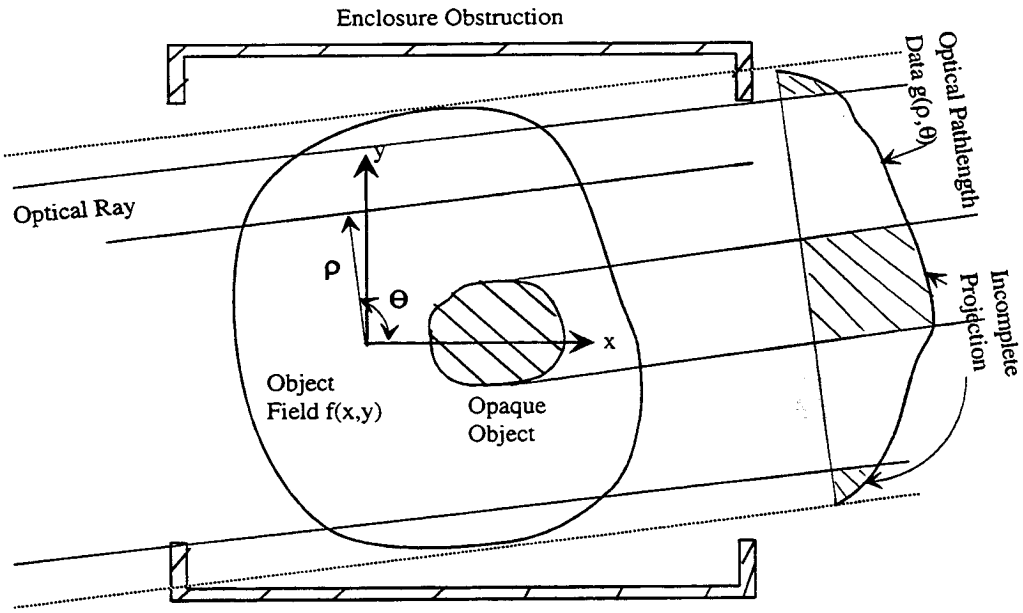

Figure 1. A typical test configuration and nomenclature for interferometric tomography.

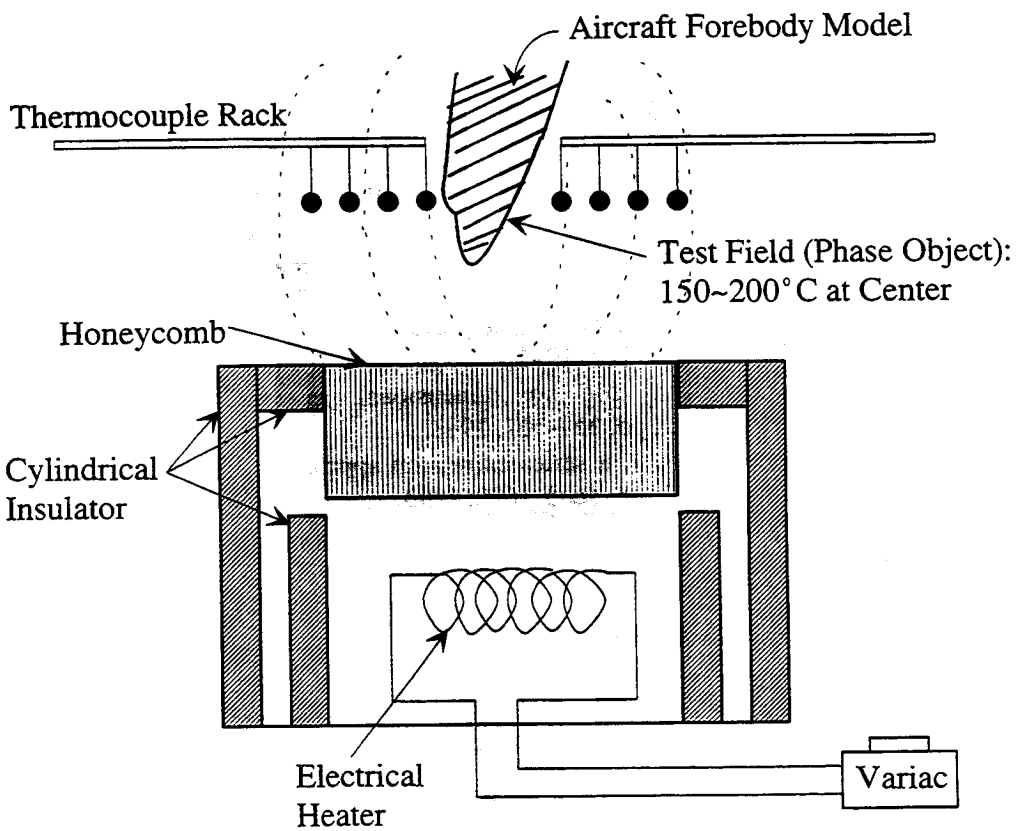

Figure 2. Test-field setup.

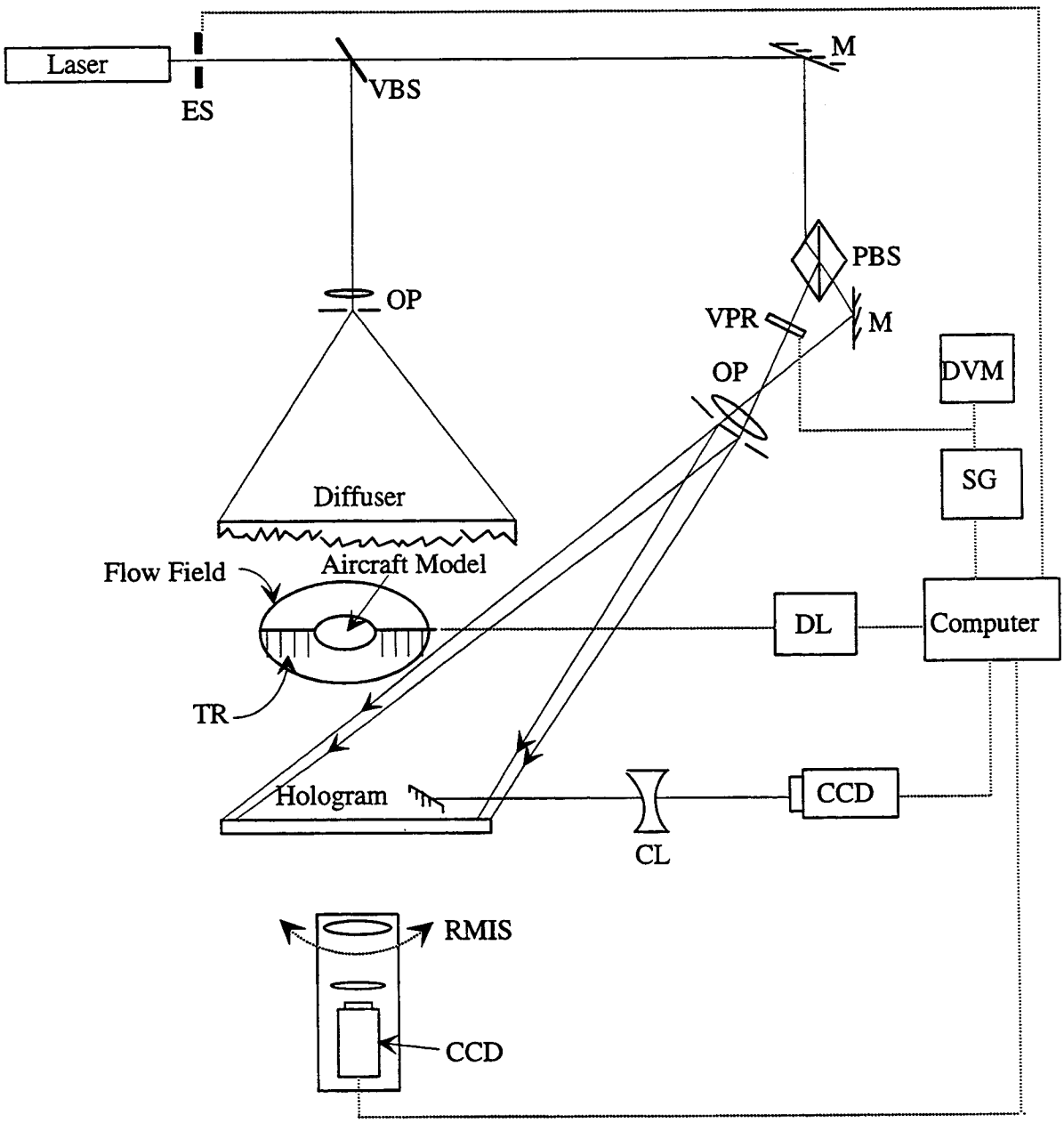

CL: cylindrical lens
DL: data logger
DVM: digital volt meter
ES: electronic shutter
M: mirror
OP: objective-pinhole assembly
PBS: prism beam spitter
RMIS: rotary rail-mounted imaging system
SG: signal generator
TR: thermocouple rake
VBS: variable beam splitter
VPR: variable phase retarder

Figure 3. The experimental arrangement.

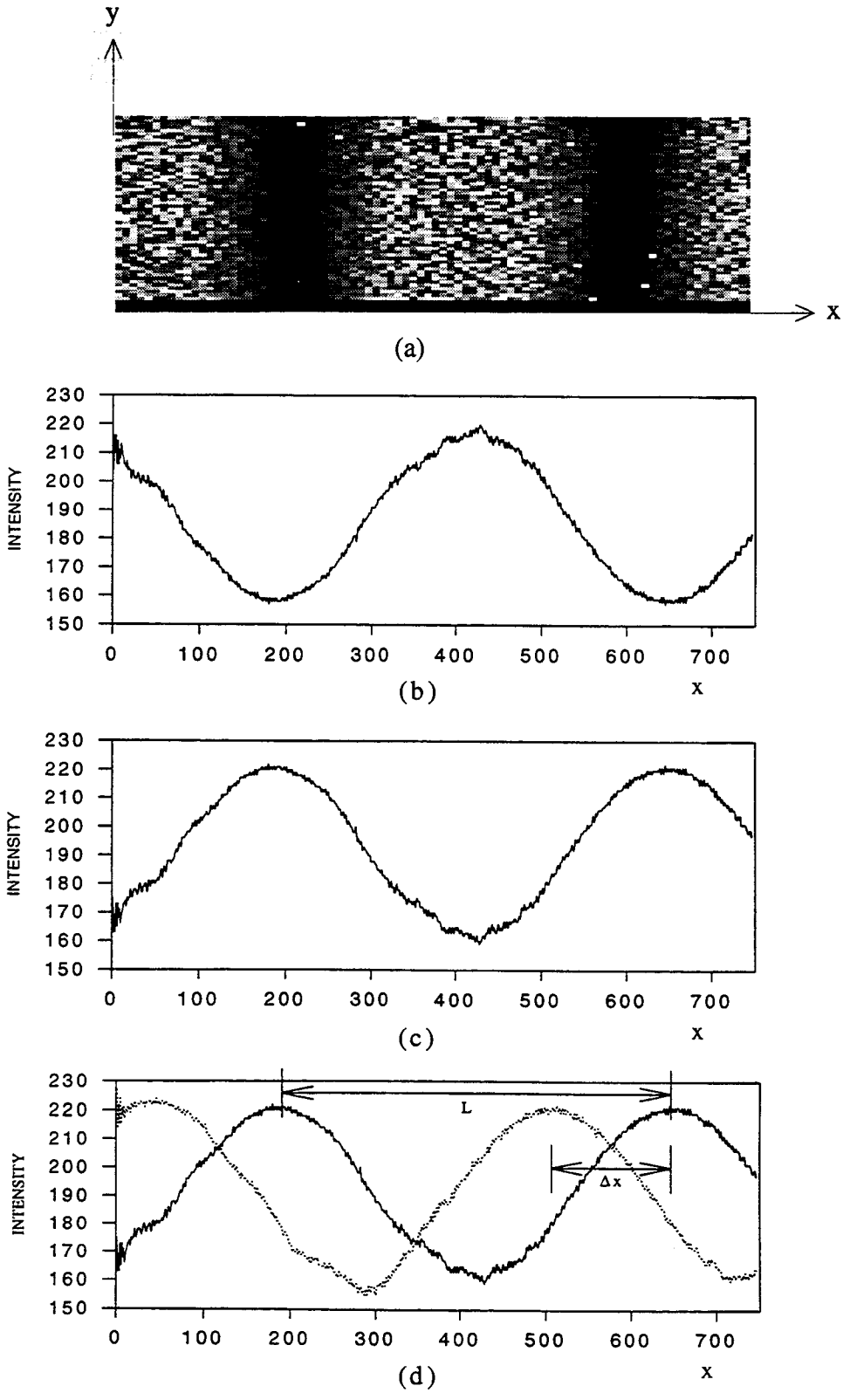

Figure 4. Extraction of phase-stepping from Young's fringes.

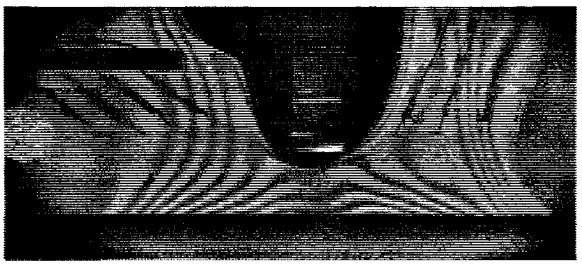

(a) $\Delta\varphi_1=0.0^0$

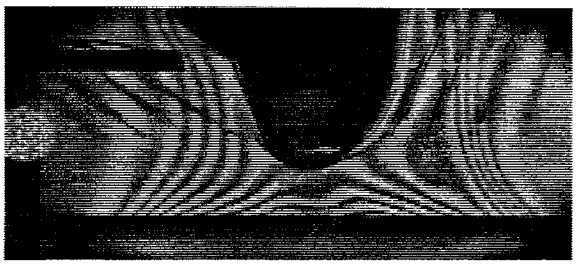

(b) $\Delta\varphi_2=-97.7^0$

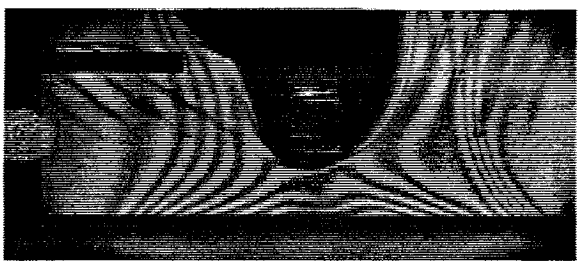

(c) $\Delta\varphi_3=-198.0^0$

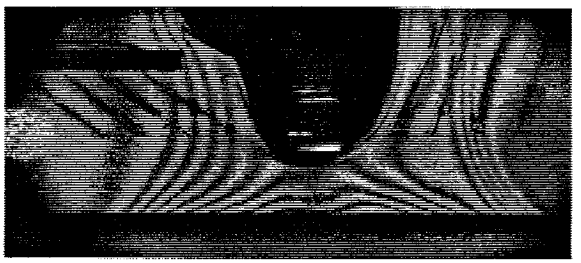

(d) $\Delta\varphi_4=-288.3^0$

Figure 5. Four phase-stepped interferograms at $\theta=90^0$.

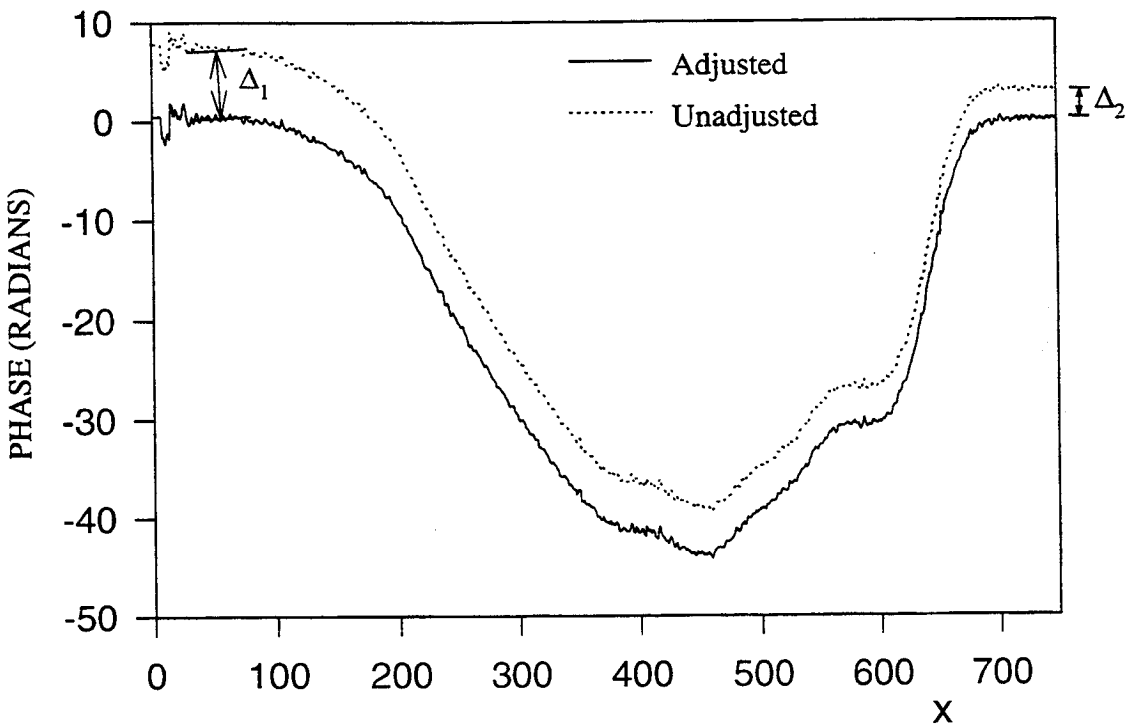

Figure 6. Unwrapped phase distribution.

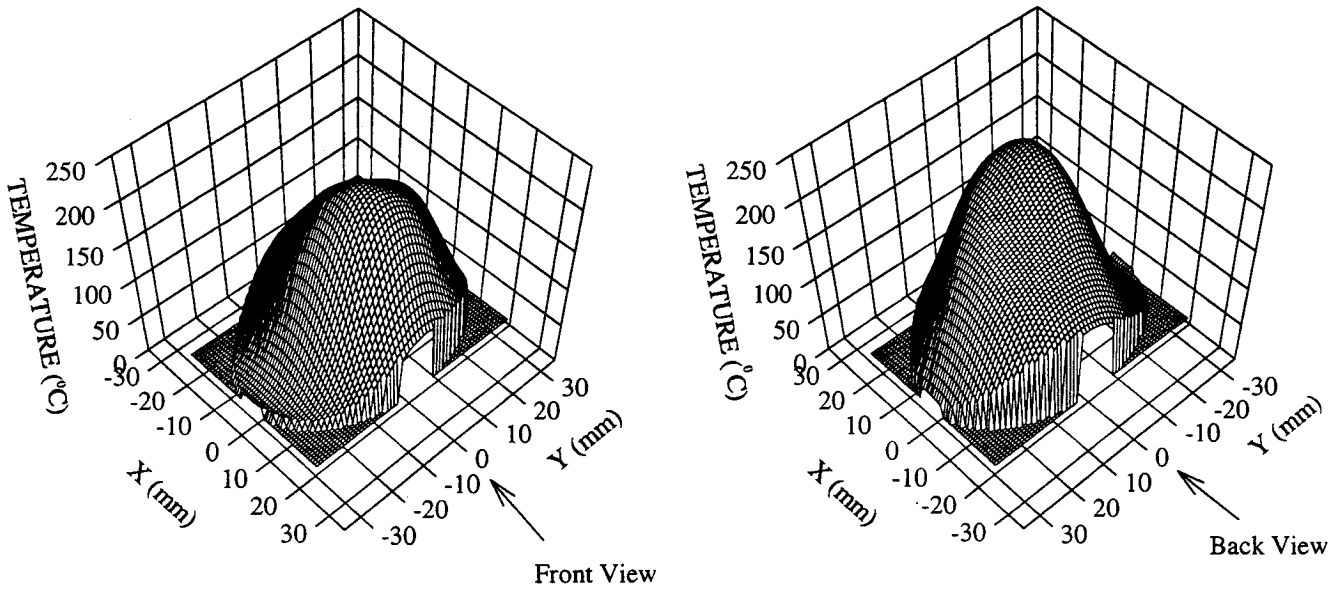

Figure 7. Reconstructed cross-section of the temperature field at 9.5 *mm* above the flow generator surface.

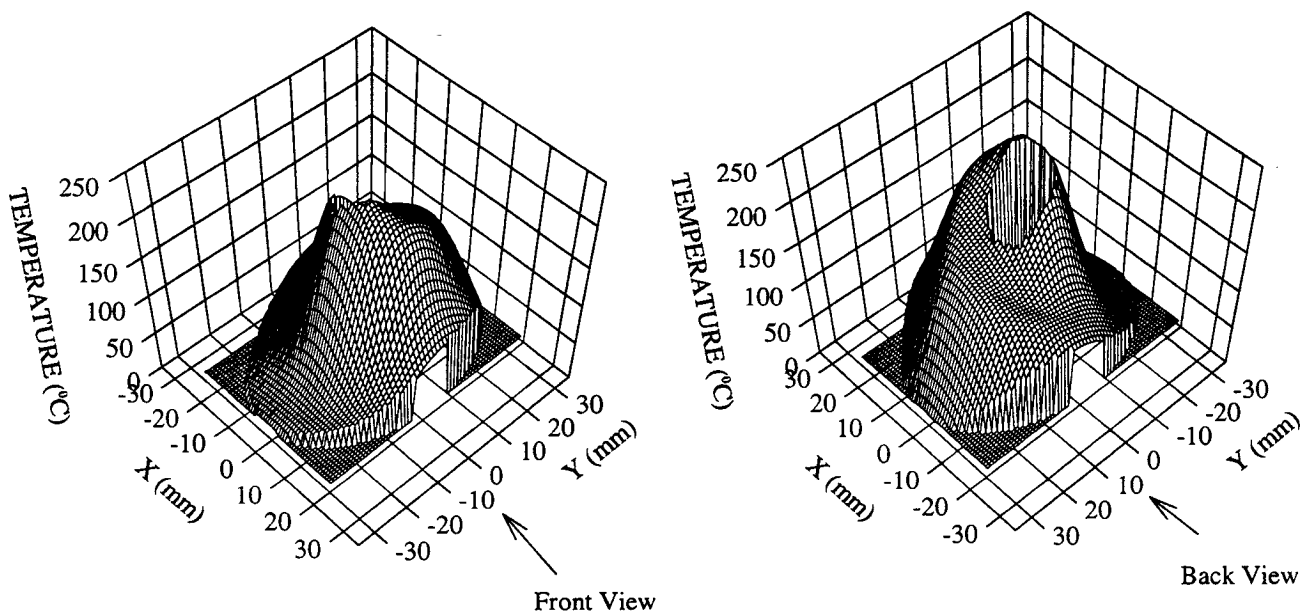

Figure 8. Reconstructed cross-section of the temperature field with the opaque test model just below the thermocouple rakes.